RSC Advances

ROYAL SOCIETY OF CHEMISTRY

www.rsc.org/advances

Journal Name

COMMUNICATION

Ultra-tiny $Co(OH)_2$ particles supported on graphene oxide for highly efficient electrocatalytic water oxidation

Received 00th January 20xx,
Accepted 00th January 20xx

DOI: 10.1039/x0xx00000x

www.rsc.org/

Jiong Liu[a,b], Fuping Du[a], Haojie Zhang[a], Chao Lin[a], Peng Gao[a], Yuyun Chen[a], Zhifang Shi[a], Xiaopeng Li[a,*], Tiejun Zhao[a,*] and Yuhan Sun[a,c]

Here, we report a novel highly efficient cobalt-based catalyst for the oxygen evolution reaction (OER), which is ~2 nm $Co(OH)_2$ clusters supported on the graphene oxide ($Co(OH)_2$/GO). Compared with hydrothermally treated Co_3O_4/GO (HT-Co3O4/GO) reported in the literature, $Co(OH)_2$/GO shows comparable OER performance but with 42% less cobalt loading mass. The turnover frequency (TOF) of $Co(OH)_2$/GO is 2.8 times as high as that of HT-Co_3O_4/GO. Our result presents a new opportunity for researchers to design efficient OER electrocatalysts.

In renewable energy technologies, the development of durable and highly efficient electrocatalysts that can convert water into oxygen, and *vice versa*, is of pivotal importance.[1-3] The bottleneck of electrochemical water splitting is the oxygen evolution reaction (OER) with sluggish reaction kinetics.[4] So far heterogeneous OER electrocatalysts mainly include transitional metal oxides such as RuO_2, IrO_2, PtO_2, MnO_2, and Co_3O_4.[5] Although the most active catalysts are the scarce noble metal oxides such as RuO_2, IrO_2 and PtO_2, there are constant interests in developing cost-effective OER catalysts based on earth-abundant metals. Co_3O_4 is slightly less active than the noble metal oxides for electrocatalytic water oxidation in alkaline solution.[5] Therefore, different techniques and strategies have been employed to further improve the electrochemical activity of cobalt oxides, such as particle size reduction,[6] specific morphological design,[7] alloying with other foreign metal elements[8, 9] and hybrid with conductive carbon materials.[10, 11]

Since the report by Dai et al.,[11] hybrid cobalt oxides with conductive graphene and its derivatives especially has been considered as one of the most promising routes to promote the electrochemical activity of cobalt oxides due to several advantages: I. Graphene has a theoretical surface area up to 2630 m^2/g. It can act as an ideal support to disperse fine catalytic metal oxide particles. Moreover, its unique two-dimensional lamellar structure allows full surface accessibility to the electrolyte. II. Graphene and its oxides contain abundant oxygenated functional groups, such as epoxides and hydroxyl on the basal plane and carbonyl and carboxyl groups at the edges. These oxygenated groups can act as nucleation sites for metal ions to form ultra-fine metal oxide nanoparticles on graphene materials. III. Conductive graphene materials can effectively compensate the poor conductivity of metal oxides. IV. The formed metal-carbon bonds can generate synergistic effects resulting in the remarkable enhancement of the electrochemical activity of the composite electrocatalysts.[12-14] Therefore, many studies have been carried out to utilize graphene and its derivatives as the support of Co_3O_4 nanoparticles as the catalyst for ORR,[11] OER,[11] and degradation of orange II in water.[15]

In this report, we started with graphene oxide (GO) and firstly synthesized the reference samples including Co_3O_4/GO and hydrothermal treated Co_3O_4/GO (HT-Co_3O_4/GO) according to the typical recipe reported in the reference [11]. Through tuning the preparation conditions, we successfully obtained a new type of cobalt based GO nanocomposite electrocatalyst. The cobalt based particle size is as small as ~ 2 nm. According to the FT-IR and XPS data, the cobalt particle phase was confirmed as $Co(OH)_2$. The $Co(OH)_2$/GO exhibited slightly higher OER performance in comparison with the reference samples while the cobalt loading mass is 36-42% less. The turnover frequency (TOF) of $Co(OH)_2$/GO is 2.8 times as high as that of HT-Co_3O_4/GO.

To obtain Co_3O_4/GO nanocomposite electrocatalyst, commonly used methods involve the precipitation of cobalt ions on GO under alkaline conditions (ammonia solution), followed by calcination or hydrothermal treatment at high temperature in early literatures.[11, 16-18] Detailed preparation procedures are described in the experimental section. Fig. 1(a-d) shows cobalt oxide nanoparticles before and after hydrothermal treatment. Nanoparticles are densely distributed on the GO surface as shown in the transmission electron microcopy (TEM) images in Fig. 1 (a) and (c). The average

[a] CAS Key Laboratory of Low-Carbon Conversion Science and Engineering, Shanghai Advanced Research Institute, Chinese Academy of Sciences, Shanghai 201412, PR China.
[b] University of Chinese Academy of Sciences, Beijing 100049, PR China.
[c] Institute of Coal Chemistry, Chinese Academy of Sciences, Taiyuan 030001, China.
Email: lixp@sari.ac.cn, zhaotj@sari.ac.cn

nanoparticles size increases from 3.3 nm to 6.9 nm after hydrothermal treatment (see inset pictures of Fig. 1(a) and (c)).

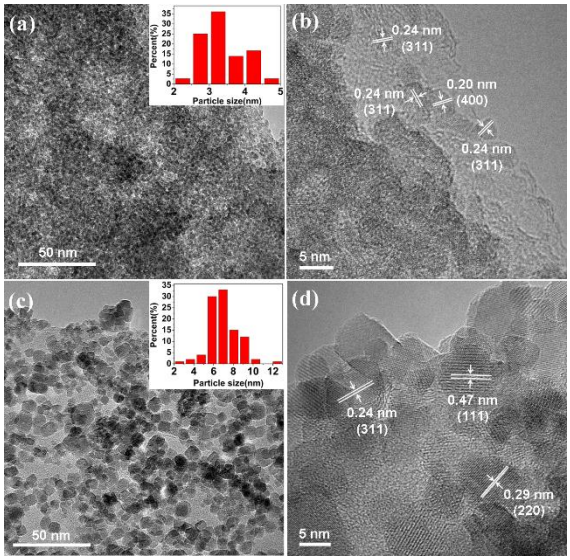

Figure 1. TEM images of (a) Co_3O_4/GO and (c) HT-Co_3O_4/GO. (b) and (d) are the corresponding HRTEM images. The inset pictures in (a) and (c) are particle-size distribution diagrams.

The high-resolution TEM (HRTEM) image clearly shows the crystalline nature (seen in Fig. 1(b) and (d)). The interplanar distances with the d-spacings of 0.20 nm, 0.24 nm, 0.29 nm, and 0.47 nm correspond to the (400), (311), (220), and (111) facets of spinel Co_3O_4, respectively.[19]

The ultra-tiny cobalt-based nanoparticle/GO was obtained via reducing the precipitation temperature to 0 ℃ and decreasing the cobalt ion concentration. A large number of small crystal nucleus will

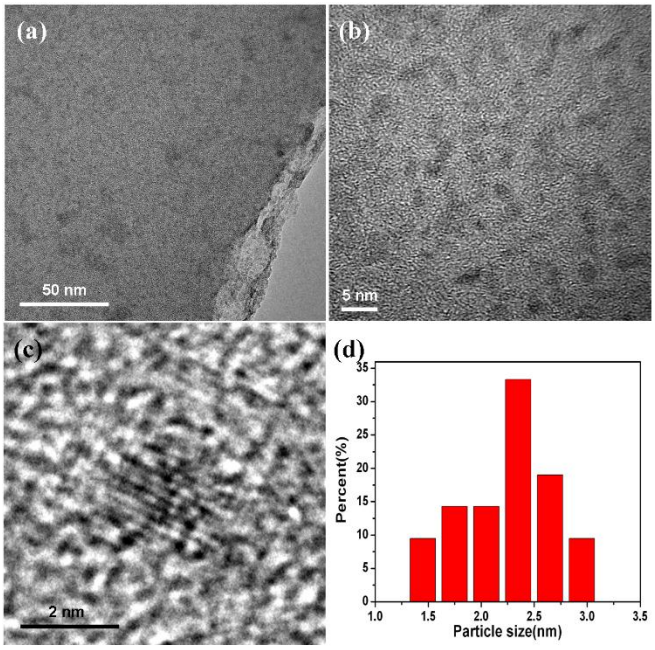

Figure 2. (a), (b) and (c) are TEM image and HRTEM images of $Co(OH)_2$/GO. (d) is particle-size distribution diagram of $Co(OH)_2$/GO.

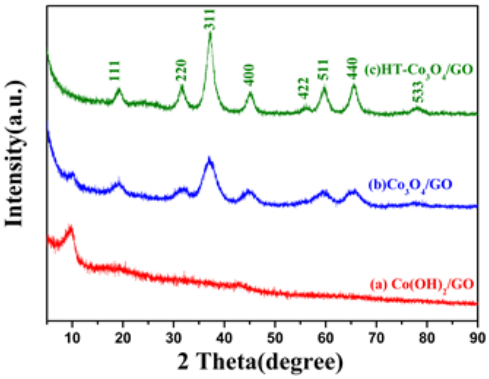

Figure 3. XRD spectra of (a) $Co(OH)_2$/GO (red), (b) Co_3O_4/GO (blue), and (c) HT-Co_3O_4/GO (Olive).

form at low temperature once the solution system reaches the precipitation threshold,[20] while low cobalt ion concentration ca stop the further growth of crystal nucleus. Fig. 2 (a,b) shows th nanoparticles are uniformly distributed all over the GO surfaces. The HRTEM image shown in Fig. 2(c) reveals the crystalline nature of the nanoparticles. The average diameter of nanoparticles is 2.2 nm (see Fig. 2(d)). However, the actual average diameter is slightly less than 2.2 nm, because it has been observed that the cobalt-based nanoparticles grew slowly after exposing to high energy electron beam in the TEM.

The phases of the aforementioned samples were firstly investigated by XRD measurements. The XRD patterns of the GO, Co_3O_4/GO and HT-Co_3O_4/GO are presented in Fig. S1 and Fig. 3. GO shows a diffraction peak at 10.06° corresponding to the (001) plane,[21] an additional small and low broad (002) diffraction peak appears at 2θ of 19.90° (see supporting information Fig. S1), which can be indexed to the disorderedly stacked graphene sheets.[16] The (001) plan reflection peak of GO also appears in the XRD pattern of Co_3O_4/GO (Fig. 3(b)), all other diffraction peaks can be ascribed to the well-crystallized Co_3O_4 with a face-centered cubic structure (fcc, *Fd3m* (227), a=0.808 nm, JCPDS No.42-1467).[16] Compared to the XRD pattern of Co_3O_4/GO, the (001) plane reflection peak of GO disappears for HT-Co_3O_4/GO (Fig. 3), indicating partial reduction of GO after the hydrothermal treatment. However, the ultra-tiny cobalt-based nanoparticle/GO sample only shows a diffraction peak at 10.06° corresponding to the (001) plane of GO. No appearances of other diffraction peaks confirms that the formed nanoparticles are extremely small less than 5 nm.

In order to further evaluate the phase and functional groups of nanocomposites, all samples were characterized by FT-IR spectroscopy. As shown in Fig. 4, the ultra-tiny cobalt-based nanoparticle/GO sample demonstrates a unique absorption band at 617 cm^{-1} can be ascribed to the formation of $Co(OH)_2$.[22, 23] In terms of both Co_3O_4/GO and HT-Co_3O_4/GO samples, two distinct and sharp absorption bands at 661-664 cm^{-1} and 576-577 cm^{-1} are owing to the formation of Co_3O_4.[15, 21, 24-27] The broad bands at 3324-3406 cm^{-1} belong to stretching vibrations of hydroxyl groups which is related to the adsorbed water and carboxy of graphene oxide.[28] A significant red-shift of O-H band to 3324 cm^{-1} can be attributed to the formation of CoO-H (Fig. 4b) which again verifies the phase of $Co(OH)_2$. It is also

worthy to note that GO also goes through chemical changes after deposition of Co_3O_4 and $Co(OH)_2$. The absorption peaks of carboxy group (C=O) and hydroxyl group (C-OH) at 1735 cm^{-1} and 1226 cm^{-1}, are missing after cobalt deposition, indicating that GO was partially reduced in the alkaline precipitation solution.

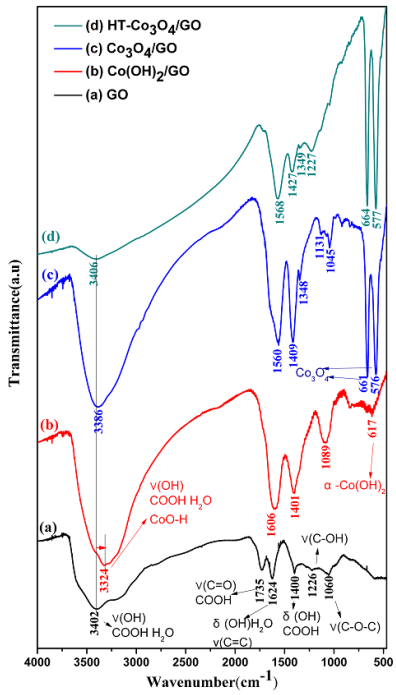

Figure 4. FT-IR spectra of (a) GO (black), (b) $Co(OH)_2$/GO (red), (c) Co_3O_4/GO (blue), and (d) HT-Co_3O_4/GO (olive).

X-ray photoelectron spectroscopy (XPS) measurements were carried out to analyse the phase, chemical components and valence of nanocomposite electrocatalysts in further detail. As seen in Fig. 5(a), the wide scan spectra of the nanocomposites demonstrates photoelectron lines at binding energies (BE) of ~285, 530 and 780 eV, corresponding to C 1s, O 1s and Co 2p, respectively. As indicated in Fig. 5(b), two strong peaks are centered at BE of ~780 and ~796 eV for all samples, which are in agreement with the BE of Co $2p_{3/2}$ and Co $2p_{1/2}$, respectively.[26] In the XPS spectra of Co_3O_4/GO and HT-Co_3O_4/GO (Fig. 5b), the Co $2p_{3/2}$-Co $2p_{1/2}$ splitting of approximately 15 eV and the shake-up satellite structure of the Co $2p_{3/2}$ at ~9 eV higher than the main peaks are associated with the Co_3O_4.[26, 29] $Co(OH)_2$/GO shows peaks at 780.2, 785.8, 796.3, and 802.3 eV which match the Co 2p peaks of $Co(OH)_2$ reported in early literatures[30-32] (Fig. 5b) and in turn confirm the FT-IR data.

The state of GO in the nanocomposites is analysed by the C 1s spectra in detail shown in Fig. 5(c). The spectrum of the C 1s spectra can be deconvoluted into five components including C=C sp^2 (284.0 eV), C–C sp^3 (284.8 eV), C–OH and/or C–O–C (286.4 eV), C=O (287.8 eV) and O–C=O (289.2 eV).[33-36] In the C 1s spectra, the intensity of C–OH and C–O–C peak is higher than that of the C=C sp^2 peak, indicating that GO is highly oxidized and contains lots of hydroxyl and epoxy groups in comparison with the carbonyl and carboxylate groups.

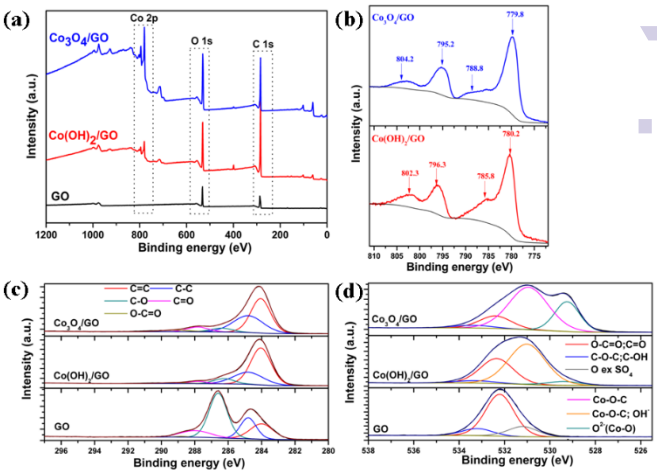

Figure 5. (a) Wide scan XPS spectra and (b) high resolution Co 2p spectra of Co_3O_4/GO, $Co(OH)_2$/GO, respectively. XPS curve fit of (c) C 1s and (d) O 1s spectra of GO, Co_3O_4/GO and $Co(OH)_2$/GO, respectively.

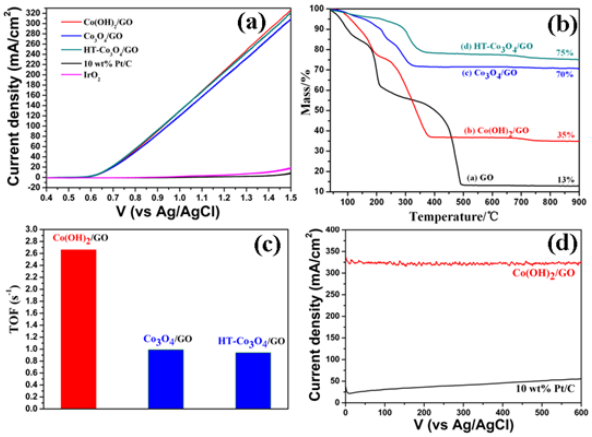

Figure 6. (a) OER polarization curves of $Co(OH)_2$/GO, Co_3O_4/GO, HT-Co_3O_4/GO, commercial 10 wt% Pt/C and IrO_2 (Sigma-Aldrich). The linear scanning rate is 50 mv/s. (b) TG curves of GO, $Co(OH)_2$/GO, Co_3O_4/GO and HT-Co_3O_4/GO in air atmosphere. (c) Histogram of TOF (detailed calculations of TOF are presented in the Supporting Information). (d) OER stability test of $Co(OH)_2$/GO and 10 wt% Pt/C under constant applied potential of 1.5 V (vs. Ag/AgCl).

After deposition of $Co(OH)_2$ or Co_3O_4, the atomic ratio of oxygenated functional groups decreased, particularly for C–OH and C–O–C (see Fig. 5(c)). These results clearly suggest that GO undergoes partial reduction due to partial removal of epoxide and hydroxyl groups, which were deoxygenated under alkaline conditions during preparation of nanocomposites. The total atomic concentrations of C=C and C-C for $Co(OH)_2$/GO and Co_3O_4/GO are 85.6 % and 84.1 %, respectively. Therefore, we can conclude that even though the preparation temperature for $Co(OH)_2$/GO is 80 ℃ lower than that for Co_3O_4/GO. The reduction level of GO for both samples is similar.

Fig. 5(d) shows the O 1s spectra of GO, $Co(OH)_2$/GO and Co_3O_4/GO, HT-Co_3O_4/GO. The deconvoluted O 1s spectra of the original GO consists of three peaks: (I) the O element in carboxylate and/or carbonyl (O–C=O; C=O: 532.2 eV), and (II) the O element in the epoxy

and/or hydroxyl (C–O–C; C–OH: 533.2 eV), (III) the O element that binds to the trace sulphate group (O ex SO_4: 531.2 eV).[37] After deposition of Co_3O_4 and $Co(OH)_2$, the O1s peak shifted to lower BE and broadened. For Co_3O_4/GO, the major reason of such shift is partial reduction of GO, the emerging peak of lattice oxygen in Co_3O_4 (Co–O: 529.4 eV) and the formation of Co–O–C bonds (~531.0 eV).[26,31] For $Co(OH)_2$/GO, the weak lattice oxygen peak at 529.4 eV again confirms the phase of $Co(OH)_2$, and the major peak at 531.0 eV can be ascribed to the OH group in $Co(OH)_2$ and the formation of Co–O–C bonds (~531.0 eV).

We tested the OER catalytic activity of $Co(OH)_2$/GO, Co_3O_4/GO, HT-Co_3O_4/GO, commercial 10 wt% Pt/C, and IrO_2 (see Fig. 6(a)). The $Co(OH)_2$/GO sample shows slightly higher performance than Co_3O_4/GO and HT-Co_3O_4/GO. In comparison with commercial noble metal electrocatalysts including 10 wt% Pt/C and IrO_2, all cobalt based GO nanocompsite electrocatalysts demonstrate overwhelming advantages. In order to evaluate the actual cobalt loading mass in GO, we conducted thermogravimetric (TG) analysis of all nanocomposite samples in the air atmosphere (see Fig. 6(b)). The final residual ratio is 35 % for $Co(OH)_2$/GO, 70 % for Co_3O_4/GO and 75 % for HT-Co_3O_4/GO. Based on the TG data, we calculated the real cobalt oxide/hydroxide loading mass ratio in nanocomposites (calculation details seen in the supporting information). The loading ratio is 30 wt% for $Co(OH)_2$/GO, much less than 66 wt% for Co_3O_4/GO and 72 wt% for HT-Co_3O_4/GO. We further evaluated the intrinsic activity of $Co(OH)_2$/GO, Co_3O_4/GO, and HT-Co_3O_4/GO, via calculating the turnover frequency (TOF) at 1.5 V (vs. Ag/AgCl) (see Fig. 6(c)). The TOF values of Co_3O_4/GO and HT-Co_3O_4/GO are 0.99 and 0.94 s^{-1}, respectively. On contrast, the TOF value for $Co(OH)_2$/GO is 2.66 s^{-1}, which is 2.7 times higher than that of Co_3O_4/GO. Considering the reduction level of GO for both samples are similar, we ascribed such high electrochemical activity of $Co(OH)_2$/GO to the extremely small size of $Co(OH)_2$ nanoparticles. The ultra-high surface-to-volume ratio of $Co(OH)_2$ nanoparticles allows the exposing huge number of active sites catalyzing the OER. Moreover, we also measured the OER stability of $Co(OH)_2$/GO. As shown in Fig. 6(d), it shows no degradation in the strong alkaline condition under the constant applied potential of 1.5 V (vs. Ag/AgCl).

In summary, we have successively prepared ~2 nm $Co(OH)_2$ clusters supported on GO. Such $Co(OH)_2$/GO electrocatalyst demonstrates slightly higher OER performance than recent intensively studied Co_3O_4/GO and HT-Co_3O_4/GO, while the loading mass of catalytic cobalt for $Co(OH)_2$/GO is 36% less than Co_3O_4/GO and 42% less than HT-Co_3O_4/GO. The turnover frequency (TOF) of $Co(OH)_2$/GO is 2.8 times as high as that of HT-Co_3O_4/GO. Moreover, it also shows perfect OER stability in the strong alkaline electrolyte. We believe our approach can be generalized to other carbon materials and applied in various areas such as supercapacitor and lithium ion battery while minimizing the metal loading amount.

References

1 H. B. Gray, *Nat. Chem.*, 2009, **1**, 7.
2 T. R. Cook, D. K. Dogutan, S. Y. Reece, Y. Surendranath, T. S. Teets and D. G. Nocera, *Chem. Rev.*, 2010, **110**, 6474.
3 S. Park, Y. Shao, J. Liu and Y. Wang, *Energ. Environ. Sci.*, 2012, **5**, 9331.
4 M. G. Walter, E. L. Warren, J. R. McKone, S. W. Boettcher, Q. Mi, E. A. Santori and N. S. Lewis, *Chem. Rev*, 2010, **110**, 6446.
5 S. Trasatti, *Electrochimica Acta*, 1984, **29**, 1503.
6 A. J. Esswein, M. J. McMurdo, P. N. Ross, A. T. Bell and T. D. Tilley, *J. Phys. Chem. C*, 2009, **113**, 15068.
7 H. Tüysüz, Y. Hwang, S. Khan, A. Asiri and P. Yang, *Nano Res.*, 2013, **6**, 47.
8 H. Y. Wang, Y. Y. Hsu, R. Chen, T. S. Chan, H. M. Chen and B. Liu, *Adv. Energy Mater.*,2015,DOI:10.1002/aenm.201500091.
9 Z. Peng, D. Jia, A. M. Al-Enizi, A. A. Elzatahry and G. Zheng, *Adv. Energy Mater.*, 2015, DOI: 10.1002/aenm.201402031.
10 X. Lu and C. Zhao, *J. Mater. Chem. A*, 2013, **1**, 12053.
11 Y. Liang, Y. Li, H. Wang, J. Zhou, J. Wang, T. Regier and H. Dai, *Nat. Mater.*, 2011, **10**, 780.
12 A. Lerf, H. Y. He, M. Forster and J. Klinowski, *J. Phys. Chem. B*, 1998, **102**, 4477.
13 D. A. C. Brownson, D. K. Kampouris and C. E. Banks, *Chem. Soc. Rev.*, 2012, **41**, 6944.
14 D. R. Dreyer, S. Park, C. W. Bielawski and R. S. Ruoff, *Chem. Soc. Rev.*, 2010, **39**, 228.
15 P. Shi, R. Su, F. Wan, M. Zhu, D. Li and S. Xu, *Appl. Catal. B-Environ*, 2012, **123**, 265.
16 Z. S. Wu, W. Ren, L. Wen, L. Gao, J. Zhao, Z. Chen, G. Zhou, F. Li and H. M. Cheng, *ACS Nano*, 2010, **4**, 3187.
17 L. Tao, J. Zai, K. Wang, H. Zhang, M. Xu, J. Shen, Y. Su and X. Qian, *J. Power Sources*, 2012, **202**, 230.
18 H. Kim, D. H. Seo, S. W. Kim, J. Kim and K. Kang, *Carbon*, 2011, **49**, 326.
19 C. H. Kuo, W. Li, W. Song, Z. Luo, A. S. Poyraz, Y. Guo, A. W. K. Ma, S. L. Suib and J. He, *Acs Appl. Mat. Interfaces*, 2014, **6**, 11311.
20 F. Schüth, M. Hesse and K. K. Unger, Precipitation and Coprecipitation, in Handbook of Heterogeneous Catalysis, 2nd Edition, Weinheim: Wiley-VCH Press, 2008.
21 D. Zhang and W. Zou, *Curr. Appl. Phys*, 2013, **13**, 1796.
22 Y. C. Zhu, H. L. Li, Y. Koltypin and A. Gedanken, *J. Mater. Chem*, 2002, **12**, 729.
23 Z. P. Xu and H. C. Zeng, *Chem. Mater.*, 1999, **11**, 67.
24 J. Xie, H. Cao, H. Jiang, Y. Chen, W. Shi, H. Zheng and Y. Huang, *Anal. Chim. Acta*, 2013, **796**, 92.
25 C. W. Tang, C. B. Wang and S. H. Chien, *Thermochim. Acta*, 2008, **473**, 68.
26 R. Xu and H. C. Zeng, *Langmuir*, 2004, **20**, 9780.
27 Z. P. Xu and H. C. Zeng, *J. Mater. Chem*, 1998, **8**, 2499.
28 M. Acik, C. Mattevi, C. Gong, G. Lee, K. Cho, M. Chhowalla and Y. J. Chabal, *ACS Nano*, 2010, **4**, 5861.
29 L. Lv, Y. Su, X. Liu, H. Zheng and X. Wang, *J. Alloy. Compd.*, 2013, **553**, 163.
30 J. A. Koza, C. M. Hull, Y. C. Liu and J. A. Switzer, *Chem. Mater.*, 2013, **25**, 1922.
31 J. Yang, H. Liu, W. N. Martens and R. L. Frost, *J. Phys. Chem. C*, 2010, **114**, 111.
32 T. Shaochun, S. Vongehr, W. Yang, C. Lan and M. Xiangkang, *J. Solid State Chem.*, 2010, **183**, 2166.
33 W. Chen, S. Li, C. Chen and L. Yan, *Adv. Mater.*, 2011, **23**, 5679.
34 N. A. Zubir, C. Yacou, J. Motuzas, X. Zhang and J. C. Diniz da Costa, *Sci. rep.*, 2014, **4**, 4594.
35 W. Fan, W. Gao, C. Zhang, W. W. Tjiu, J. Pan and T. Liu, *J. Mater. Chem.*, 2012, **22**, 25108.
36 Z. J. Fan, W. Kai, J. Yan, T. Wei, L. J. Zhi, J. Feng, Y. M. Ren, L P. Song and F. Wei, *ACS Nano*, 2011, **5**, 191.
37 D. Rosenthal, M. Ruta, R. Schlogl and L. Kiwi-Minsker, *Carbon*, 2010, **48**, 1835.